Nano-impact Electrochemistry

How to cite:
International Edition: doi.org/10.1002/anie.202207270
German Edition: doi.org/10.1002/ange.202207270

From Ensemble Electrochemistry to Nano-Impact Electrochemistry: Altered Reaction Selectivity

Rui Zhong, Xiaoyu Wang, Qianqian Tao, Jianhua Zhang, Chuhong Lin, Hui Wei,* and Yi-Ge Zhou**

Abstract: Selective electrochemical production of valued chemicals is of significant importance but remains a great challenge in chemistry. Conventional approaches for enhancing reaction selectivity focus on the improvement of the catalysts themselves. In this work, we systematically studied the reaction kinetics and mass transport behavior of $LaNiO_3$ nanocubes ($LaNiO_3$ NCs) catalyzed hydrogen peroxide reduction reaction (HPRR) at ensemble and single nanoparticle levels using nano-impact electrochemistry (NIE). We find that the selectivity of HPRR was altered at individual random-walk nanoparticles as compared to their ensemble counterpart without changing the reaction kinetics, due to the significantly enhanced mass transport at single nanoparticles. This discovery offers the scope of new catalytic approaches for engineering electrochemical reactions in general.

Introduction

Selective electrochemical synthesis of the desired and valued products is of particular significance in chemistry. Recently, extensive attentions have been paid to improving the reaction selectivity of a variety of reactions, in which the electrochemical CO_2 reduction for CO production,[1–4] CO electrocatalytic reduction to form multi-carbon products,[5,6] H_2O_2 electrogeneration by oxygen reduction reaction[7,8] and the electrosynthesis of NH_3 from N_2 reduction[9,10] are important representatives. Main strategies to enhance the reaction selectivity have been focused on the improvement of the catalysts themselves before they are modified on the electrode, including surface engineering,[6,11] doping modification[12–15] and defect construction.[16] However, these approaches usually require rather complex reagents or sophisticated protocols. In addition, the resulting catalysts may also promote other reaction pathways, resulting in unsatisfying selectivity enhancement.

Single nanoparticle electrochemistry, different from the electrochemistry of nanoparticles supported on an electrode, is able to unveil the intrinsic properties of individual nanoparticles masked in the ensemble-averaged measurements.[17] Among single nanoparticle electrochemistry, nano-impact electrochemistry (NIE) is currently an active technique based on the stochastic collisions of individual nanoparticles onto an inert ultramicroelectrode, which has been utilized to probe a variety of single nanoparticles[18–20] and biological entities.[21] NIE-based reaction mode has been found to significantly increase the reaction efficiency by enhancing the mass transport of reactants.[22–25] Furthermore, since the spatial and temporal continuum of the reaction at ensemble electrochemistry is broken, this mode can also accelerate reaction kinetics[22] and minimize catalyst degradation.[25]

In this work, we find that NIE enabled single nanoparticle electrochemistry can also alter the reaction selectivity by using $LaNiO_3$ nanocubes (NCs) catalyzed hydrogen peroxide reduction reaction (HPRR) as a model reaction. $LaNiO_3$ NC is a member of perovskite oxides displaying high electrocatalytic activity towards HPRR, which was reported to very possibly take place through a direct electrochemical reaction mechanism of H_2O_2 (direct HPRR) and a chemical electrochemical reaction mechanism including a chemical decomposition of H_2O_2 to O_2 followed by an electrochemical oxygen reduction reaction (ORR).[26] The ORR involved indirect reaction pathway is not desired in HPRR, because it is a slow four-electron transfer process compared to the faster two-electron reduction of the direct HPRR.[27] Moreover, the generation of the oxygen bubbles may decrease the active surface area of the electrode and intensify the fuel crossover problem under the context of a fuel cell application.[26–28] Herein, by combining experiments and theoretical simulations, the reaction kinetics and mass

[*] R. Zhong, J. Zhang, Prof. Y.-G. Zhou
Institute of Chemical Biology and Nanomedicine (ICBN), State Key Laboratory of Chemo/Biosensing and Chemometrics, College of Chemistry and Chemical Engineering, Hunan University
Changsha, 410082 (P. R. China)
E-mail: yigezhou@hnu.edu.cn

X. Wang, Prof. H. Wei
Department of Biomedical Engineering, College of Engineering and Applied Sciences, Nanjing National Laboratory of Microstructures, Jiangsu Key Laboratory of Artificial Functional Materials, Chemistry and Biomedicine Innovation Center (ChemBIC), Nanjing University
Nanjing, 210023 (China)
E-mail: weihui@nju.edu.cn

Dr. C. Lin
School of Chemical and Biomedical Engineering, Nanyang Technological University
62 Nanyang Drive, Singapore, 637459 (Singapore)
E-mail: chuhonglin92@gmail.com

Q. Tao, Prof. H. Wei
State Key Lab of Analytical Chemistry for Life Science, School of Chemistry and Chemical Engineering, Nanjing University
Nanjing, 210023 (China)

transport behavior of $LaNiO_3$ NCs catalyzed HPRR were systematically studied at ensemble level and single nanoparticle level using nano-impact electrochemistry. Interestingly, the current ratio of the direct HPRR to the ORR was found to increase by *ca.* five times at the voltammogram equivalent to a single nanoparticle compared to ensemble electrochemistry without changing the reaction kinetic parameters, indicating that much improved reaction selectivity can be obtained at single nanoparticles. This should be attributed to the significantly enhanced mass transport at single nanoparticles over their ensemble counterpart. This work highlights the improvement of reaction selectivity enabled by individual random-walk nanoparticles and provides new insight in the design of catalyst working mode in electrochemical systems.

Results and Discussion

Our previous study has demonstrated that e_g is an effective activity descriptor for the design of peroxidase-like nanozymes by using ABO_3 (where A is a rare-earth or alkaline-earth metal and B is a transition metal) perovskite oxides as a model system (Figure 1a).[29] Optimized by e_g descriptor, $LaNiO_3$ with a peroxidase-like activity 1–2 orders of magnitude higher than that of other representative metal oxide-based and carbon-based nanozymes can be obtained. To characterize the morphology of the as-prepared $LaNiO_3$ nanozymes, transmission electron microscopy (TEM) and scanning electron microscopy (SEM) measurements were performed, showing a cube structure with a size of about 400 nm (Figure 1b and Figure S1). The high-resolution TEM image in Figure 1c exhibits the magnified $LaNiO_3$ matrix with well-defined lattice fringes, where the d-spacing of 0.271 nm corresponds to the (110) crystal planes of $LaNiO_3$ perovskite. The elemental distribution was then obtained by HAADF-STEM characterization coupled with EDS elemental mapping (Figure 1d), which shows uniform distribution of La, Ni, and O in $LaNiO_3$ NCs. To further reveal the structural information, X-ray diffraction patterns are shown in Figure 1e, suggesting that the obtained product presents typical diffraction peaks of the $LaNiO_3$ perovskite structure without the crystalline phases of lanthanum or nickel oxides. As shown in Figure S2, the as-prepared $LaNiO_3$ NCs exhibits excellent peroxidase-like activity, following the typical Michaelis–Menten curve. The electrochemical characterization of the $LaNiO_3$ NCs was carried out by performing cyclic voltammogram (CV) at a bare glassy carbon (GC) electrode and a $LaNiO_3$ NCs modified GC electrode in a 0.1 M KOH solution in the scan range of 1 V to 1.7 V (vs. RHE), shown in Figure 1f. It can be seen that a redox couple appears at 1.3 V and 1.45 V, respectively, corresponding to the redox cycle of Ni^{4+}/Ni^{3+}, which is consistent with the prior observations.[26,30]

Before investigating HPRR at $LaNiO_3$ NCs ensembles, a $LaNiO_3$ NCs modified GC electrode was first scanned in the potential range of 1 V to −0.5 V in a N_2-saturated solution of 0.1 M KOH without the presence of H_2O_2 at a scan rate of 50 mV s^{-1} (Figure 2a, blue, dashed lines) to allow the study of the intrinsic electrochemical property of $LaNiO_3$ NCs. It is found that a distinct cathodic current at 0.3 V in the first cycle was observed, attributing to the reduction of Ni^{3+} to Ni^{2+},[30] while no reduction feature was shown on a bare GC electrode (black line). In the backward scan, no oxidative behavior exhibited, suggesting that Ni^{3+} reduction to Ni^{2+} is an irreversible reaction. This is due to a little destruction of the crystal structure induced in the reductive process, where Ni^{2+} ions produced is unable to occupy their

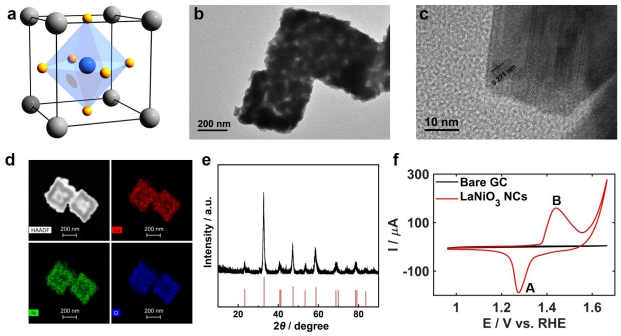

Figure 1. Characterization of $LaNiO_3$ NCs. a) Schematic illustration of ABO_3 perovskite structure. A (rare earth or alkaline-earth metal), B (transition metal), and O are shown in gray, blue, and yellow, respectively. TEM image (b) and high-resolution TEM image (c) of $LaNiO_3$ NCs. d) The elemental mapping of La, Ni, O for $LaNiO_3$ NCs. e) Powder X-ray diffraction patterns of the $LaNiO_3$ NCs. f) CVs of a bare GC electrode (black line) and a $LaNiO_3$ NCs modified GC electrode (red line) in a 0.1 M KOH solution at a scan rate of 50 mV s^{-1}.

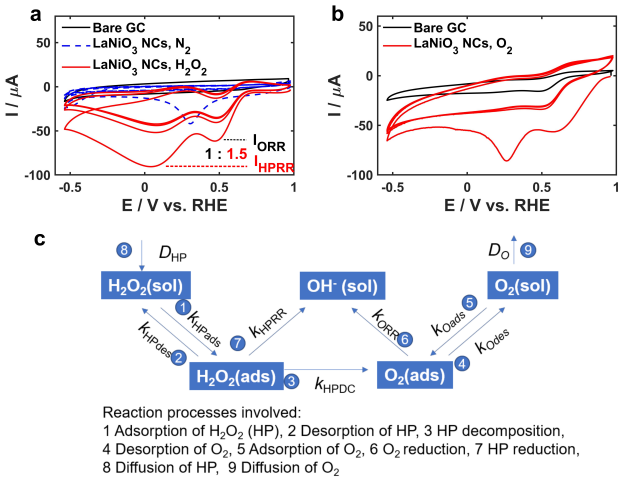

Figure 2. HPRR catalyzed by $LaNiO_3$ NCs ensembles. a) CV of a bare GC electrode (black line) in a N_2 saturated 0.1 M KOH solution at a scan rate of 50 mV s^{-1}; multiple-scan CVs of a $LaNiO_3$ NCs modified GC electrode in a N_2-saturated 0.1 M KOH solution with (red line) and without (blue, dashed line) 10 mM H_2O_2 at a scan rate of 50 mV s^{-1}. I_{ORR} and I_{HPRR} refer to the peak currents of ORR and direct HPRR. Background current of the H_2O_2 CV was removed. b) CV of a bare GC electrode (black line) and multiple-scan CVs of a $LaNiO_3$ NCs modified GC electrode (red line) in a O_2-saturated 0.1 M KOH solution. c) Elementary steps and kinetic parameters of the HPRR mechanism.

original sites without any deformation of the lattice.[30] In addition, the subsequent scans show no further reduction peaks, indicating that the reduction of the surface Ni^{3+} can be completed in the first cycle. Followig that, HPRR at the $LaNiO_3$ NCs modified GC electrode was studied in the same potential range in a N_2-saturated solution of 0.1 M KOH containing 10 mM H_2O_2 in Figure 2a (red line). Compared with a flat curve observed at the bare GC electrode (data very similar to that in N_2-saturated 0.1 M KOH without H_2O_2, which is not shown), two well-defined reduction peaks at ca. 0.5 V and 0 V, respectively, were obtained at the $LaNiO_3$ NCs modified GC electrode.

As was mentioned previously, $LaNiO_3$ catalyzed HPRR includes a direct electrochemical reduction of H_2O_2 (direct HPRR) and an oxygen reduction reaction (ORR) following the chemical decomposition of H_2O_2 to form oxygen.[26] In order to explore the attribution of the two reductive peaks for HPRR, CVs in the potential range of 1 V to −0.5 V were repeated at a $LaNiO_3$ NCs modified GC electrode (red) and a bare GC electrode (black) in an oxygen saturated 0.1 M KOH solution, shown in Figure 2b. It is found that in the first CV cycle, two obvious reduction peaks were clearly seen at ca. 0.5 V and 0.3 V, respectively. Previous studies indicate that the former should be due to ORR at $LaNiO_3$.[31] Therefore, the peak at 0.5 V in Figure 2a is attributed to the electrochemical reduction of the oxygen coming from the chemical decomposition of H_2O_2. The other reduction peak at 0 V for HPRR should then be corresponding to the direct HPRR. The peak at 0.3 V in Figure 2b is attributed to the irreversible reduction of Ni^{3+} to Ni^{2+}, which disappeared in the subsequent scans.

It is noticed that the reduction peaks at 0 V for $LaNiO_3$ NCs catalyzed HPRR in Figure 2a show a significant decrease in the later scans as compared to the first scan. Given that the reduction of Ni^{3+} to Ni^{2+} for surface $LaNiO_3$ only contributes a minor part, we speculated that the decrease in the current might be due to mass transport limitation of H_2O_2 with increasing reaction time in the later scans. This assumption was later proved both in theory and experiments. It is also observed that the ratio of the current peak for the direct HPRR to that for ORR is about 1.5:1.

To find out the reaction kinetics and mass transport information involved in HPRR catalyzed by $LaNiO_3$ NCs ensembles, a theoretical model of the ORR and the direct HPRR at $LaNiO_3$ NCs supported on a GC electrode was built, as shown in Figure 2c. The 9 kinetic processes and the corresponding reaction rate constants/diffusion coefficients involved in the model were also listed in Figure 2c, where k_{HPads} (unit: $mM^{-1}s^{-1}$) and k_{HPdes} (unit: s^{-1}) are the adsorption and desorption rate constants of H_2O_2; k_{HPDC} (unit: s^{-1}) is the decomposition rate constant of H_2O_2; k_{Oads} (unit: $mM^{-1}s^{-1}$) and k_{Odes} (unit: s^{-1}) are the adsorption and desorption rate constants of O_2; k_{ORR} (unit: s^{-1}), $E_{f,ORR}$ (unit: V) and α_{ORR} are the rate constant, the formal potential and the transfer coefficient of the ORR, respectively; k_{HPRR}, $E_{f,HPRR}$ and α_{HPRR} are those of the direct HPRR, respectively. Since the reduction current of $Ni^{3+/2+}$ was much lower than that of the direct HPRR and the reduction reaction only occurred at the first time using the $LaNiO_3$ NCs modified electrode for its irreversibility, the reduction of Ni^{3+} to Ni^{2+} was ignored in the simulation for simplicity.

Detailed reaction equations of Figure 2c can be found in Supporting Information, Equations (S1) to (S5). As we mainly investigated the influence of H_2O_2 adsorption, H_2O_2 decomposition and H_2O_2 mass transport on the selectivity of HPRR, the detailed, stepwise chemical and electrochemical mechanism of ORR and HPRR were not considered in this model. The electrochemical reaction rate was assumed to follow the Butler–Volmer equation. The diffusion coefficients of O_2 and H_2O_2 were assumed to be $2.0\times10^{-9}\ m^2s^{-1}$ according to the previous reports.[32,33] We assumed that the adsorption of H_2O_2 and O_2 competed with each other on the $LaNiO_3$ surface. The values of Γ_{max} (surface coverage of total active sites for both H_2O_2 and O_2), which relates to the catalytic property of the electrode material, and other kinetic variables (k_{HPads}, k_{HPdes}, k_{Oads}, k_{Odes}, k_{HPDC}) were determined by fitting to the experimental CVs. The formal potentials of the ORR and the direct HPRR with adsorbate reactants O_2(ads) and H_2O_2(ads) were determined by both the formal potentials of O_2(sol) and H_2O_2(sol) (1.23 V vs. RHE and 0.78 V vs. RHE in the solution of 0.1 M KOH, respectively)[34] and the corresponding thermodynamic adsorption equilibrium coefficients, see Supporting Information, Equations (S10) and (S11).

Since a macro-sized electrode modified with close-packed nanoparticles is equivalent to a macroelectrode made up of the same material as the nanoparticles,[35] we treated the $LaNiO_3$ NCs modified GC electrode as a $LaNiO_3$ macroelectrode in the following simulation. For the simulation on a macro-sized electrode, the edge effect can be ignored and the diffusion follows the mode of "linear diffusion".[36] However, when the size of the electrode decreases from millimeter to the level of micrometer or even nanometer, as the edge curvature cannot be neglected, the diffusion becomes "radial diffusion".[36] The diffusion of solution-phase H_2O_2 and O_2 was described by the Fick's second law for both macroelectrode and single nanoparticles. By solving the partial differential equations [Supporting Information, Equations (S12) and (S13)] with the boundary conditions of Equations [Supporting Information, Equations (S6)–(S9) and (S14), (S15)], the concentration/surface coverage profiles of H_2O_2 and O_2 were calculated. A home-made program was built for the simulation and data analysis was performed in Matlab 2020b.

The selecitivity of HPRR is defined as the ratio of peak currents (macroelectrode) or steady-state currents (single NP) between HPRR and ORR, I_{HPRR}/I_{ORR}. Figure 3 predicts the theoretical selectivity under the influence of H_2O_2 adsorption (ADS), H_2O_2 decomposition (DC) and H_2O_2 mass transport (MT, which is determined by the interplay between the active site surface coverage Γ_{max} and the diffusion ability). The variables affecting HPRR selectivity include not only the kinetic parameters listed in Figure 2c but also the active site surface coverage Γ_{max}, the concentration of bulk H_2O_2 c_{HP}*, the scan rate v or the nanoparticle radius r_{NP}. To simplify the analysis, the influence of each kinetic parameters and Γ_{max} on HPRR selectivity was evaluated in Figure S3, where k_{HPads}, k_{HPDC}, D_{HP}, Γ_{max} (only

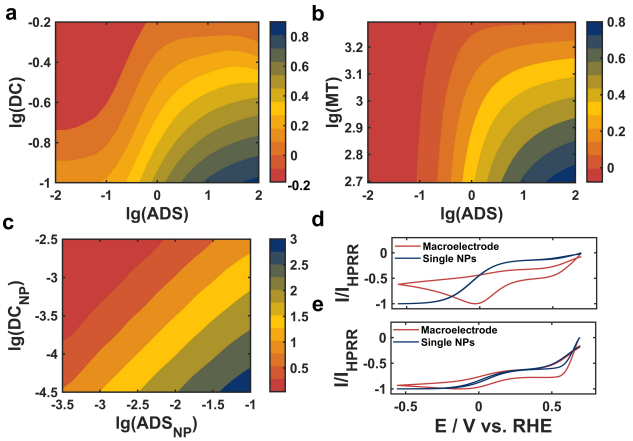

Figure 3. Selectivity (I_{HPRR}/I_{ORR}) as a function of combined kinetic parameters. a) Selectivity diagram of macroelectrodes over H_2O_2 adsorption (ADS) and H_2O_2 decomposition (DC) rates, ADS = $k_{HPads}c^*_{HP}RT/\nu F$, DC = $k_{HPDC}RT/\nu F$. b) Selectivity diagram of macroelectrodes over ADS and H_2O_2 mass transport (MT) rates, ADS = $k_{HPads}c^*_{HP}RT/\nu F$, MT = $\Gamma_{max}/\left(c^*_{HP}\sqrt{D_{HP}RT/\nu F}\right)$. c) Selectivity diagram of single nanoparticles (NPs) over ADS and DC rates, ADS_{NP} = $k_{HPads}c^*_{HP}r^2_{NP}/D_{HP}$, DC_{NP} = $k_{HPDC}r^2_{NP}/D_{HP}$. Simulated CVs of a macroelectrode (radius 1.5 mm) and a single NP (radius 200 nm) with d) relatively strong H_2O_2 adsorption (k_{HPads} = 2.5 s^{-1}) and f) weak H_2O_2 adsorption (k_{HPads} = 0.25 s^{-1}), where other simulation parameters were identical as Figure S3, c_{HP}* = 10 mM and ν = 50 mV s^{-1}.

for macroelectrodes) were found to mainly determine the selectivity of HPRR and were considered in the simulation. In addition, the local pH effect was not considered in the theory. Though local pH may differ from the bulk value, the selectivity should not vary much, which was proved in Figure S4 where the pH difference only shifts the overpotential of the direct HPRR and ORR as a whole without causing noticeable change in the HPRR selectivity. The key variables as well as the experimental conditions c_{HP}*, ν and/or r_{NP} were further combined into three dimensionless factors: ADS, DC and MT (two dimensionless factors of ADS_{NP} and DC_{NP} for single NPs, as less kinetic variables are needed). ADS, DC and MT indicate the contribution from H_2O_2 adsorption, H_2O_2 decomposition and the sufficiency of H_2O_2 mass transport compared to the material active site density. ADS_{NP} and DC_{NP} refer to the H_2O_2 adsorption and decomposition compared to the mass transport of H_2O_2. The definition of the combined parameters is listed in the caption of Figure 3. Figure 3a and b show the simulated selectivity under the linear diffusion mode (macroelectrode) as a function of ADS, DC and MT. On a macroelectrode, increasing the H_2O_2 concentration is helpful to improve the selectivity as it increases ADS and decreases MT; increasing the mass transport of H_2O_2 improves the selectivity only when the reaction is not limited by a slow ADS ($ADS > 10^{-1}$); increasing the active site density of the material may lead to a decrease in HPRR selectivity when ADS is not slow ($ADS > 10^{-1}$), as a large Γ_{max} is favourable for other competing surface reactions; increasing the scan rate decreases the values of ADS and DC but increases MT, which usually leads to a slight improvement on the selectivity. Note that the selectivity diagram is not the same as the activity diagram and the same variation in experiment may lead to different response on selectivity and activity. For instance, increasing Γ_{max} improves the current but decreases the selectivity, as shown in Figure S3h.

Compared to the macroelectrodes, the selectivity diagram on single NPs are relatively simple. Figure 3c shows the simulated selectivity under the radial diffusion mode as a function of ADS_{NP} and DC_{NP}. Increasing the concentration of H_2O_2 can also increase the selectivity, but the selectivity is independent of the variation of D_{HP} and r_{NP} in the case of radial diffusion. Figure S5 shows that the selectivity on single NPs is also independent of Γ_{max}, indicating that slight size variation of NPs due to agglomeration or synthesis difference will not affect the HPRR selectivity. The selectivity difference between the macroelectrode and single NPs is due to different mass transport efficiency between linear diffusion and radial diffusion. The more significantly the reaction is limited by slow mass transport of reactants, the more the HPRR selectivity will be improved after switching from the macroelectrode to single NPs. It is worth noting that the rate of H_2O_2 adsorption plays a role in the selectivity. Figure 3d shows the simulated CVs of a macroelectrode (red) and a single NP (blue) under the case of a moderate H_2O_2 adsorption, where I_{HPRR}/I_{ORR} is 2 for the macroelectrode but 4 for the single NP. In contrast, the simulated CVs under the case of a slow H_2O_2 adsorption displayed in Figure 3e gives a I_{HPRR}/I_{ORR} very similar to both electrodes. These results indicate that the change in the diffusion mode can alter the selectivity of reactions in which adsorption is not the rate-determining step.

The theoretical prediction was verified by fitting to experimental CVs recorded on a $LaNiO_3$ NCs modified GC electrode with a radius of 1.5 mm. By fitting to experimental CVs, the values of the kinetic parameters (k_{HPads}, k_{HPdes}, k_{Oads}, k_{Odes}, k_{HPDC}, k_{ORR}, k_{HPRR}) used in the simulation were determined, which can be found in Figures S3. Figure 4a shows the experimental (black, dashed lines) and the simulated (blue, solid lines) CVs with H_2O_2 concentrations c_{HP}* of 2, 5, 10, 20 mM. Figure 4b shows the experimental (black, dashed lines) and the simulated (blue, solid lines) CVs with scan rates ν of 20, 50, 100, 200 mV s^{-1}. Similar to the prediction of selectivity diagrams, I_{HPRR}/I_{ORR} increases with both c_{HP}* and ν. When simulating to the variation of c_{HP}*, we found that the decomposition rate constant k_{HPDC} is

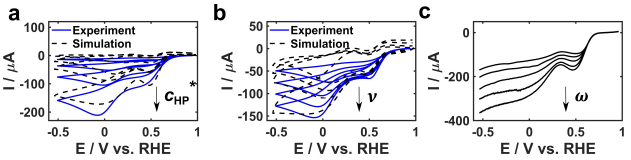

Figure 4. Influence of HP mass transport on $LaNiO_3$ NCs modified GC electrode. a) CVs of various HP concentrations c_{HP}*. c_{HP}* = 2, 5, 10 and 20 mM. b) CVs of various scan rates ν:ν = 20, 50, 100, 200 mV s^{-1}. c) CVs at a rotating disk electrode of various stirring speeds ω:ω = 100, 200, 400, 900, 1600 rpm. For simulation CVs in (a), k_{HPDC} = 0.95 $(c_{HP}$*$)^{0.8}$ s^{-1}; other simulation parameters were identical as Figure S3. Background current was removed for all experimental CVs.

actually proportional to $(c_{HP}^*)^{0.8}$, indicating that the reaction order for H_2O_2 in the decomposition reaction rate equation [Equations (S7) and (S8)] is not 1. Therefore in the fitting to experimental data, we applied the expression of $k_{HPDC} \propto (c_{HP}^*)^{0.8}$. Comparing to the theoretical selectivity diagrams of Figure 3a, the real HPRR selectivity is less sensitive to the increase of H_2O_2 concentration. After modifying the expression of k_{HPDC}, the simulations fitted well with the experiments, proving the validation of the theoretical model. The effect of the reactant diffusion efficiency was further investigated in Figure 4c, where $LaNiO_3$ NCs were modified on a rotating disk electrode. When the rotating speed ω increases from 100 rpm to 1600 rpm, I_{HPRR}/I_{ORR} increases nearly twice, confirming that the selectivity to HPRR can be promoted by simply increasing the mass transport efficiency of the reactant. To better display the correlation of the experimental parameters to the selectivity, the calculated selectivity against the experimental parameters were plotted in Figure S6. For HPRR, the side reaction of ORR resulting from H_2O_2 decomposition is not desirable for real applications. However, the catalysts for HPRR usually also favour the decomposition of H_2O_2 and the subsequent ORR, which makes it difficult to avoid the side reaction by just improving catalytic materials themselves.[26,27,37] The combination of the theoretical modelling and experimental studies clearly suggest that the alteration of the reaction selectivity can be achieved by only changing the mass transport efficiency.

To investigate the kinetics of HPRR catalyzed by single $LaNiO_3$ NCs, nano-impact electrochemistry (NIE) was performed at a 7 μm diameter carbon ultramicroelectrode in a 0.1 M KOH solution containing 100 mM H_2O_2 and 1.1 pM $LaNiO_3$ NCs under different potentials. Figure 5a displays a segment of the high-temporal-resolution chronoamperometric profile of HPRR at 0.2 V vs RHE, where typical reductive current spikes were observed. In Figure S7, two control experiments were carried out without $LaNiO_3$ NCs present in solution (black line), or with $LaNiO_3$ NCs but under a potential of 1 V (red line), where the $LaNiO_3$ NCs are not electrochemically active for catalyzing HPRR (see Figure 2a). No current spikes were observed (Figure S7, inset) for both cases, confirming that the catalytic process of HPRR during collisions of single $LaNiO_3$ NCs with the electrode surface is the source of the current spikes. It is noteworthy that a concentration of 1.1 pM nanoparticles in NIE can well avoid multiple collision events according to the approximation using Poisson theorem based on the prior study,[38] therefore, the current spikes should be corresponding to single nanoparticle collisions. Meanwhile, as shown in Figure S8, $LaNiO_3$ NCs can maintain good dispersion stability within the NIE experimental time scale, suggesting that there should be almost no aggregates of $LaNiO_3$ NCs responsible for the current spikes. Similarly, chronoamperometric measurements at a series of potentials ranging from 0.6 V to −0.4 V vs. RHE were performed, and the corresponding impact spikes of single $LaNiO_3$ NCs catalyzed HPRR were collected, shown in Figure S9. Those electrochemical impact spikes were analyzed by a home-written data processing program, the details of which can be found in Supporting Information (Figure S10a and S10b).[39,40] The potential dependence of the resulting averaged current produced from single $LaNiO_3$ NCs is shown in Figure S10c, which is equivalent to a voltammogram of HPRR catalyzed by a single $LaNiO_3$ NC.

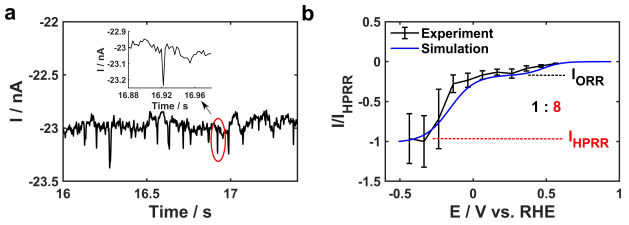

Figure 5. Nano-impact signals of single $LaNiO_3$ NCs. a) A segment of chronoapmerometric response showing reductive current transients at the potential of 0.2 V. The inset shows close-up view of a representative current spike; b) Comparison between the potential dependent experimental average nano-impact current response and the simulated CV at a single $LaNiO_3$ NC. Simulated currents were normalized by the HPRR steady state current I_{HPRR}. Simulation parameters were identical with Figure S3.

We also simulated the voltammogram of a single $LaNiO_3$ NC attaching to the electrode surface, where a spherical nanoparticle model was applied to simplify the calculation. The corresponding current response of a single $LaNiO_3$ NC can be calculated by solving the partial differential equations [Supporting Information, Equations (S12) and (S13)] under a spherical coordinate.[41] Note that the kinetics variables applied in the single nanoparticle model were identical with those used for macroelectrode simulation and the same expression of $k_{HPDC} = 0.95(c_{HP}^*)^{0.8}\,s^{-1}$ was applied for c_{HP}^* equal to 100 mM. The kinetic parameters obtained from the CVs of the macroelectrode fitted well with the electrochemcial response of single NPs, confirming the theoretical model in Figure 2c and eliminating the possibility of other significant kinetic effect such as the variation of local pH when changing from the macroelectrode to single NPs. Since the absolute current value measured from impact experiments was filtered by the potentiostat and our data processing program, the absolute current value obtained from the chronoamperometric curves cannot be directly compared to the simulated current. As we mainly discussed the selectivity of HPRR at single $LaNiO_3$ NCs, we normalized both the experimental and the simulated currents by their steady-state currents I_{HPRR} (the current value at high overpotentials).

The corresponding normalized experimental voltammogram for single $LaNiO_3$ NCs (black, dashed line with error bars) and the simulated voltammogram (blue, solid line) for an attached $LaNiO_3$ NC are shown in Figure 5b. It is observed that the experimental current response exhibits two plateaus: the one at ca. 0.4 V vs. RHE corresponding to ORR and the other at ca. −0.3 V vs. RHE corresponding to direct HPRR. The same plateaus can also be found in the simulated CV, which agrees well with the experimental data in the tendency of the current change with potential. From the nanoparticle ensembles modified macroelectrode to the single nanoparticle, all the kinetic parameters are identical and the only difference between the two systems lies in the

diffusion mode of the reactant, i.e., linear diffusion at a macroelectrode and a much more efficient convergent/radial diffusion at a single nanoparticle. The ratio of the direct HPRR current to the ORR current at a single $LaNiO_3$ NC was observed to be ca. 8 (Figure 5b), which is 5 times higher than that at the $LaNiO_3$ NCs ensembles (Figure 2a), suggesting that the electrochemistry of the individual random-walk $LaNiO_3$ NCs can significantly improve the selectivity of HPRR by enhancing the mass transport of H_2O_2.

Conclusion

In conclusion, by combining experiments and theoretical simulations, we studied the reaction kinetics and mass transport behavior of H_2O_2 electroreduction reaction (HPRR) catalyzed by $LaNiO_3$ NCs in an ensemble and nano-impact manner. It is found that the reaction selectivity can be altered at individual random-walk nanoparticles without changing the reaction kinetics between the two manners, which should be due to the significantly enhanced mass transport at single nanoparticles over their ensemble counterpart. This discovery highlights the improvement of the reaction selectivity enabled by the electrochemistry of the individual random-walk nanoparticles. Meanwhile, it offers the scope of new catalytic approaches to be developed.

Acknowledgements

This work was supported by National Natural Science Foundation of China (21972039) and the Science and Technology Project of Hunan Province (2020SK2014, 2020RC3021, 2020JJ3005).

Conflict of Interest

The authors declare no conflict of interest.

Data Availability Statement

The data that support the findings of this study are available from the corresponding author upon reasonable request.

Keywords: Hydrogen Peroxide Reduction Reaction (HPRR) · Lanio3 Naonocubes (Lanio3 NCs) · Mass Transport · Nano-Impact Electrochemistry (NIE) · Reaction Selectivity

[1] H. Zhang, J. Li, S. Xi, Y. Du, X. Hai, J. Wang, H. Xu, G. Wu, J. Zhang, J. Lu, J. Wang, *Angew. Chem. Int. Ed.* **2019**, *58*, 14871–14876; *Angew. Chem.* **2019**, *131*, 15013–15018.
[2] Y. Pan, R. Lin, Y. Chen, S. Liu, W. Zhu, X. Cao, W. Chen, K. Wu, W. C. Cheong, Y. Wang, L. Zheng, J. Luo, Y. Lin, Y. Liu, C. Liu, J. Li, Q. Lu, X. Chen, D. Wang, Q. Peng, C. Chen, Y. Li, *J. Am. Chem. Soc.* **2018**, *140*, 4218–4221.
[3] Y. Gao, F. Li, P. Zhou, Z. Wang, Z. Zheng, P. Wang, Y. Liu, Y. Dai, M. H. Whangbo, B. Huang, *J. Mater. Chem. A* **2019**, *7*, 16685–16689.
[4] Y. Ye, Y. Liu, Z. Li, X. Zou, H. Wu, S. Lin, *J. Colloid Interface Sci.* **2021**, *586*, 528–537.
[5] S. H. Lee, I. Sullivan, D. M. Larson, G. Liu, F. M. Toma, C. Xiang, W. S. Drisdell, *ACS Catal.* **2020**, *10*, 8000–8011.
[6] Y. Liu, H. Jiang, Z. Hou, *Angew. Chem. Int. Ed.* **2021**, *60*, 11133–11137; *Angew. Chem.* **2021**, *133*, 11233–11237.
[7] X. Xiao, T. Wang, J. Bai, F. Li, T. Ma, Y. Chen, *ACS Appl. Mater. Interfaces* **2018**, *10*, 42534–42541.
[8] Y. Jiang, P. Ni, C. Chen, Y. Lu, P. Yang, B. Kong, A. Fisher, X. Wang, *Adv. Energy Mater.* **2018**, *8*, 1801909.
[9] K. Chu, Q. Q. Li, Y. P. Liu, J. Wang, Y. H. Cheng, *Appl. Catal. B* **2020**, *267*, 118693.
[10] A. R. Singh, B. A. Rohr, J. A. Schwalbe, M. Cargnello, K. Chan, T. F. Jaramillo, I. Chorkendorff, J. K. Nørskov, *ACS Catal.* **2017**, *7*, 706–709.
[11] X. Feng, K. Jiang, S. Fan, M. W. Kanan, *ACS Cent. Sci.* **2016**, *2*, 169–174.
[12] T.-P. Fellinger, F. Hasché, P. Strasser, M. Antonietti, *J. Am. Chem. Soc.* **2012**, *134*, 4072–4075.
[13] Y. Sun, I. Sinev, W. Ju, A. Bergmann, S. Dresp, S. Kühl, C. Spöri, H. Schmies, H. Wang, D. Bernsmeier, B. Paul, R. Schmack, R. Kraehnert, B. Roldan Cuenya, P. Strasser, *ACS Catal.* **2018**, *8*, 2844–2856.
[14] D. Iglesias, A. Giuliani, M. Melchionna, S. Marchesan, A. Criado, L. Nasi, M. Bevilacqua, C. Tavagnacco, F. Vizza, M. Prato, P. Fornasiero, *Chem* **2018**, *4*, 106–123.
[15] S. Chen, Z. Chen, S. Siahrostami, D. Higgins, D. Nordlund, D. Sokaras, T. R. Kim, Y. Liu, X. Yan, E. Nilsson, R. Sinclair, J. K. Nørskov, T. F. Jaramillo, Z. Bao, *J. Am. Chem. Soc.* **2018**, *140*, 7851–7859.
[16] X. Li, T. Li, Y. Ma, Q. Wei, W. Qiu, H. Guo, X. Shi, P. Zhang, A. M. Asiri, L. Chen, B. Tang, X. Sun, *Adv. Energy Mater.* **2018**, *8*, 1801357.
[17] S. E. F. Kleijn, S. C. S. Lai, M. T. M. Koper, P. R. Unwin, *Angew. Chem. Int. Ed.* **2014**, *53*, 3558–3586; *Angew. Chem.* **2014**, *126*, 3630–3660.
[18] J. H. Zhang, Y. G. Zhou, *J. Electrochem.* **2019**, *25*, 374–385.
[19] X. Xiao, A. J. Bard, *J. Am. Chem. Soc.* **2007**, *129*, 9610–9612.
[20] Y. G. Zhou, N. V. Rees, R. G. Compton, *Angew. Chem. Int. Ed.* **2011**, *50*, 4219–4221; *Angew. Chem.* **2011**, *123*, 4305–4307.
[21] J. H. Zhang, Y. G. Zhou, *TrAC Trends Anal. Chem.* **2020**, *123*, 115768.
[22] M. Chen, S. M. Lu, Y. Y. Peng, Z. Ding, Y. T. Long, *Chem. Eur. J.* **2021**, *27*, 11799–11803.
[23] C. H. Lin, R. G. Compton, *Curr. Opin. Electrochem.* **2019**, *14*, 186–199.
[24] C. H. Lin, J. J. Ye, X. J. Huang, *Chem. Eng. J.* **2021**, *418*, 129393.
[25] Y. G. Zhou, Y. Kang, J. X. Huang, *CCS Chem.* **2020**, *2*, 31–41.
[26] S. J. Amirfakhri, J. L. Meunier, D. Berk, *J. Power Sources* **2014**, *272*, 248–258.
[27] J. Milikić, G. Ćirić-Marjanović, S. Mentus, D. M. F. Santos, C. A. C. Sequeira, B. Šljukić, *Electrochim. Acta* **2016**, *213*, 298–305.
[28] J. C. Shyu, C. L. Huang, *J. Power Sources* **2011**, *196*, 3233–3238.
[29] X. Y. Wang, X. J. Gao, L. Qin, C. Wang, L. Song, Y. N. Zhou, G. Zhu, W. Cao, S. Lin, L. Zhou, K. Wang, H. Zhang, Z. Jin, P. Wang, X. Gao, H. Wei, *Nat. Commun.* **2019**, *10*, 704.
[30] Y. Matsumoto, H. Yoneyama, H. Tamura, *J. Electroanal. Chem.* **1977**, *80*, 115–121.

[31] J. Hu, Q. Liu, Z. Shi, L. Zhang, H. Huang, *RSC Adv.* **2016**, *6*, 86386–86394.
[32] X. Chang, C. Batchelor-McAuley, R. G. Compton, *Chem. Sci.* **2020**, *11*, 4416–4421.
[33] S. J. Arnold, W. G. Brownlee, G. H. Kimbell, *J. Phys. Chem.* **1970**, *74*, 8–14.
[34] J. A. Dean, *Lange's Handbook of Chemistry*, 15th ed, McGrawHill, New York, **1998**.
[35] S. R. Belding, E. J. F. Dickinson, R. G. Compton, *J. Phys. Chem. C* **2009**, *113*, 11149–11156.
[36] R. G. Compton, E. Laborda, R. W. Kristopher, *Understanding Voltammetry: Simulation of Electrode Processes*, 2nd ed, World Scientific Publishing Europe Ltd, Singapore, **2013**.
[37] R. C. P. Oliveira, J. Milikić, E. Daş, A. B. Yurtcan, D. M. F. Santos, B. Šljukić, *Appl. Catal. B* **2018**, *238*, 454–464.
[38] S. M. Oja, D. A. Robinson, N. J. Vitti, M. A. Edwards, Y. Liu, H. S. White, B. Zhang, *J. Am. Chem. Soc.* **2017**, *139*, 708–718.
[39] K. Kanokkanchana, E. N. Saw, K. Tschulik, *ChemElectroChem* **2018**, *5*, 3000–3005.
[40] E. Kätelhön, E. E. L. Tanner, C. Batchelor-McAuley, R. G. Compton, *Electrochim. Acta* **2016**, *199*, 297–304.
[41] L. F. Chen, C. H. Lin, R. G. Compton, *Phys. Chem. Chem. Phys.* **2018**, *20*, 15795–15806.

Manuscript received: May 17, 2022
Accepted manuscript online: July 12, 2022
Version of record online: August 3, 2022

Research Articles

Nano-impact Electrochemistry

R. Zhong, X. Wang, Q. Tao, J. Zhang, C. Lin,* H. Wei,* Y.-G. Zhou* e202207270

From Ensemble Electrochemistry to Nano-Impact Electrochemistry: Altered Reaction Selectivity

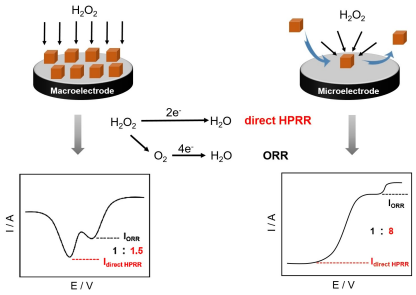

The reaction kinetics and mass transport behavior of $LaNiO_3$ nanocube (NC)-catalyzed hydrogen peroxide reduction reaction (HPRR) were systematically studied at ensemble and single nanoparticle levels. The selectivity of HPRR was altered at individual random-walk nanoparticles as compared to their ensemble counterpart without changing the reaction kinetics, offering the scope of new catalytic approaches to be developed.